

Synchronous Medical Image Augmentation framework for deep learning-based image segmentation

Jianguo Chen^{a,b}, Nan Yang^{c,*}, Yuhui Pan^b, Hailing Liu^d, Zhaolei Zhang^b

^a School of Software Engineering, Sun Yat-sen University, Zhuhai, 519082, China

^b Donnelly Centre for Cellular and Biomolecular Research, Department of Molecular Genetics and Department of Computer Science at University of Toronto, Toronto, ON M5S 3E2, Canada

^c Department of Infectious Disease, the First Affiliated Hospital of Xi'an Jiaotong University, Xi'an, Shaanxi 710061, China

^d Department of Hematology, the Second Affiliated Hospital of Xi'an Jiaotong University, Xi'an, Shaanxi 710004, China



ARTICLE INFO

Keywords:

Medical image augmentation
Deep learning
Image-label pair
Synchronous augmentation

ABSTRACT

Various deep learning (DL) models are widely applied in medical image analysis, and their performance depends on the scale and diversity of available training data. However, medical images often suffer from difficulty in data acquisition, imbalance in sample categories, and high cost of labeling. In addition, most image augmentation approaches mainly focus on image synthesis only for classification tasks, and rarely consider the synthetic image-label pairs for image segmentation tasks. In this paper, we focus on the medical image augmentation for DL-based image segmentation and the synchronization between augmented image samples and their labels. We design a Synchronous Medical Image Augmentation (SMIA) framework, which includes two modules based on stochastic transformation and synthesis, and provides diverse and annotated training sets for DL models. In the transform-based SMIA module, for each medical image sample and its tissue segments, a subset of SMIA factors with a random number of factors and stochastic parameter values are selected to simultaneously generate augmented samples and the paired tissue segments. In the synthesis-based SMIA module, we randomly replace the original tissues with the augmented tissues using an equivalent replacement method to synthesize new medical images, which can well maintain the original medical implications. DL-based image segmentation experiments on bone marrow smear and dermoscopic images demonstrate that the proposed SMIA framework can generate category-balanced and diverse training data, and have a positive impact on the performance of the models.

1. Introduction

Medical image analysis has been widely used for clinical examination and diagnosis of diseases such as tumor diagnosis, brain function testing, and cardiovascular screening (Rahim et al., 2021; Salahuddin et al., 2022). Deep Learning (DL) is a promising technology of artificial intelligence and data analysis. It has been widely used in medical imaging fields, such as lesion recognition, tissue segmentation, and medical image classification (Velden et al., 2022; Yu et al., 2022). Most DL models have the advantages of not requiring preprocessing, high accuracy, and simple model construction, the performance of which depends on the size and representativeness of the training sets. However, medical images often suffer from difficulty in data acquisition, imbalance in sample categories, and high cost of annotations, which limits the application of DL models and has a negative effect on the performance. Therefore, it is essential to generate large-scale annotated and diverse medical images as the training sets for DL models.

Image Augmentation (IA) is an effective technique to address the above challenges, which aims to expand the scale and diversity of training sets, and enhance the generalization ability of DL models (Yang et al., 2022; Guan et al., 2022). Existing IA methods can be divided into three categories, such as basic augmentation, deformable augmentation, and DL-based image augmentation (Chlap et al., 2021). Basic augmentation methods mainly include sampling, geometric, and color transformation, but usually lead to over-fitting problems (Cao et al., 2018). Deformable augmentation approaches, i.e., randomized displacement field, are applied in medical images (Chaitanya et al., 2021; He et al., 2022). In recent years, many DL-based IA methods have been presented and achieved excellent results (Chen et al., 2022). However, existing methods generally fail to adequately take into account the unique characteristics of medical images and tissues, such as tissue rotation equivalence, tissue size sensitivity, and tissue position variability. Furthermore, most of them focus on image synthesis only

* Corresponding author.

E-mail address: Shmily.1989.2008@stu.xjtu.edu.cn (N. Yang).

for classification tasks, and rarely consider the synthetic image-label pairs for image segmentation tasks.

In this paper, we focus on image augmentation for DL-based medical image segmentation task and synchronous generation of sample-label pairs. We propose a Synchronous Medical Image Augmentation (SMIA) framework that contains two stochastic transformation and synthesis modules. Experiments show that the proposed SMIA framework can provide large-scale balanced and diversified training data for DL models and improve the accuracy of the models. The contributions of this paper are summarized as follows.

- Image augmentation factor (IAF) library. We analyze the unique characteristics of medical images and serve as the theoretical basis for SMIA. On this basis, we build a SMIA factor library by collecting a series of atomic basic and deformable factors.
- Transform-based SMIA module. We design a transform-based SMIA module based on the IAF library. For each medical image and its segmentation labels, we select a stochastic combination of IAF factors to perform random transformation and synchronously generate augmented image-label pairs.
- Synthesis-based SMIA module. We further design a synthesis-based SMIA module, where an augmented tissue bank is constructed by extracting and augmenting the tissues from each original medical image. We propose an equivalent replacement method to randomly replace the original and augmented tissues in the background image, which can well preserve the original medical meaning.
- Synchronous augmentation. Both transform-based and synthesis-based SMIA modules provide synchronous augmentation, which can not only efficiently generate large-scale and diverse training datasets with medical significance, but also maintain accurate matching between samples and segmentation labels. The enhanced image can be directly used as the training set of medical image segmentation DL models without additional labeling.

The rest of the paper is organized as follows. Section 2 reviews the related work. Section 3 describes the architecture of the proposed SMIA framework and discusses the characteristics of medical images. Section 4 details the transform-based and synthesis-based SMIA modules. Experimental results and performance evaluations are discussed in Section 5. Finally, Section 6 concludes the paper with a discussion of future work and research directions.

2. Related work

Various Machine Learning (ML) and DL methods have been applied in medical image analysis of different diseases (Zhao et al., 2022; Wang et al., 2022). Medical image segmentation and classification are two main landing applications, and the corresponding examples are shown in Fig. 1. Both of them require large-scale training datasets to achieve high accuracy and performance. DL image classification models such as the Convolutional Neural Network (CNN), GoogLeNet (Szegedy et al., 2016), and ResNet (He et al., 2016), are widely used for medical image classification and disease predication. At the same time, there are many DL models available for medical image segmentation, such as SegNet (Badrinarayanan et al., 2017), RefineNet (Lin et al., 2017), and DeepLab (Chen et al., 2017). Different from DL image classification models, the training dataset of DL image segmentation models requires not only medical images as training samples, but also corresponding segmentation labels for each sample. This is a very time-consuming and highly specialized work, and it also increases the difficulty of image augmentation for image segmentation rather than classification.

Focusing on medical image augmentation, various basic, deformable, and DL-based image augmentation methods have been presented (Xu et al., 2020; Chen et al., 2020). A generative sequence model was proposed to train unlabeled data by using specified transformation functions (Ratner et al., 2017). Ranzato et al. proposed a

gated MRF method that modulates pairwise dependencies and implies pixel intensities to generate realistic images (Ranzato et al., 2010). Focusing on DL-based Data Augmentation (DA) methods, the Generative Adversarial Network (GAN) is an effective algorithm for generating large-scale training data (Frid-Adar et al., 2018a). Maayan et al. used GAN to generate synthetic medical images and applied to computed tomography (CT) images of liver lesions (Frid-Adar et al., 2018b). Xu et al. designed an enhanced framework of GANs with geometric transformation and applied in environmental microorganisms images (Xu et al., 2020). Chen et al. proposed a residual network and generative adversarial network to increase the scale of cervical single-cell images, and used the augmented dataset as the training set of a DL classification model (Chen et al., 2020). Shi et al. proposed a DA method based on cycle-consistent adversarial networks and applied to annotate image instances to generate Fluorescence Encoded Microsphere (FEM) images (Shi et al., 2019).

The existing research mainly tends to provide common image augmentation methods for all application fields, and rarely considers the unique characteristics of medical images. Although there are many traditional and DL-based augmentation methods applied to medical images, most of them are suitable for classification tasks, and rarely consider the generation of image-label pairs for image segmentation tasks. Therefore, image augmentation of DL-based medical image segmentation still faces multiple challenges.

- (1) Unique characteristics of medical images. Compared with images in other fields, medical images have multiple unique characteristics, such as scaling sensitivity, position sensitivity, and motion sensitivity for partial tissues. The size of medical organs and tissues is an important indicator to evaluate the health status of people or animals, which has important medical significance. Changing the size of organs and tissues during image augmentation will affect medical characteristics. In addition, the location of some organs or tissues has specific medical significance, but it is not always the case. Therefore, some existing image augmentation methods (i.e., shrinkage, rotation, and motion) applied in other fields cannot be directly applied to all medical images.
- (2) Image-label pairs for image segmentation DL model training. Unlike medical image classification tasks, as the training datasets of medical image segmentation DL models, we need to extract all target tissues in the training samples to form an image-label pair, and use them as the segmentation labels and ground truths. However, manual extraction and annotation tissues takes a lot of time and requires the efforts of professionals.
- (3) Imbalance of medical sample categories. Owing to the uncertainty of patient visits, many medical images from clinical applications have an imbalance in the number of samples between normal and diseased samples or between different diseases. The same phenomenon occurs in biomedical experimental applications, such as cell detection and genetic testing. Unbalanced medical images will lead to bias in ML or DL results. While some IA methods use down-sampling and up-sampling strategies to control sample category balance, they will cause over-fitting problems.

In most medical image processing applications, the above problems are inevitable, and these problems affect the application and promotion of DL methods in medical image analysis. Therefore, it is critical to provide an effective IA method to provide large-scale, category-balanced, annotated, and diverse training data for DL models based on small-scale medical image data. Different from existing approaches, we delve into the specific characteristics of medical images and tissues and serve as the theoretical basis for medical image augmentation. The SMIA framework proposed in this paper will be directly applied to medical images such as BMS images and dermoscopic images and produce augmented images that maintain the original medical implications. Furthermore, to the best of our knowledge, this is the first attempt to address the synchronization of augmented medical image samples and corresponding tissue segments and target ground truths.

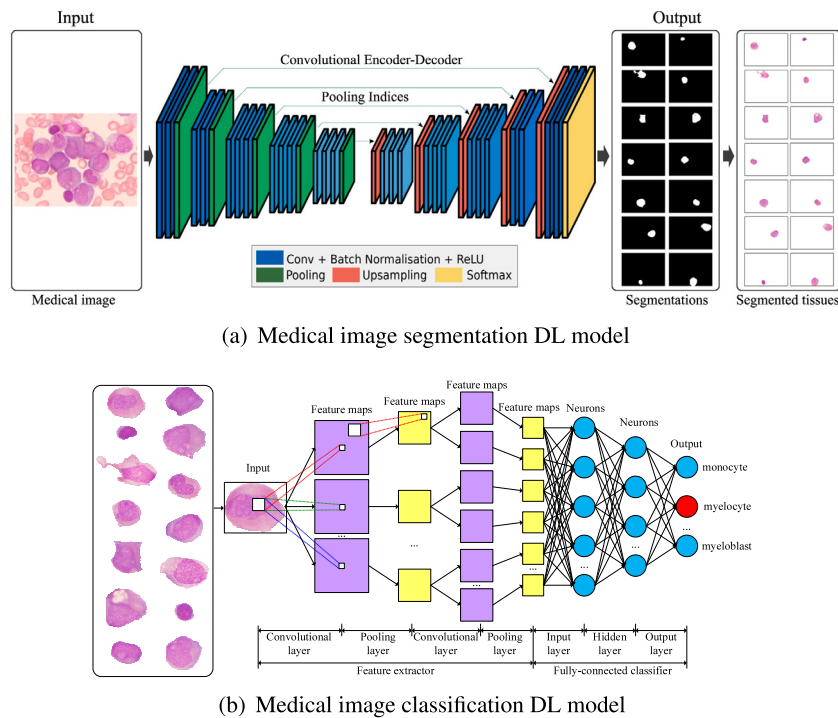


Fig. 1. Example of DL modes for medical image segmentation and classification on a BMS image. (a) is a medical image segmentation DL model, where the input is a medical image and the output are the tissue segmentation of the image. (b) is a medical image classification DL model, where the input is a medical image or tissue and the output is the corresponding name or category of the input.

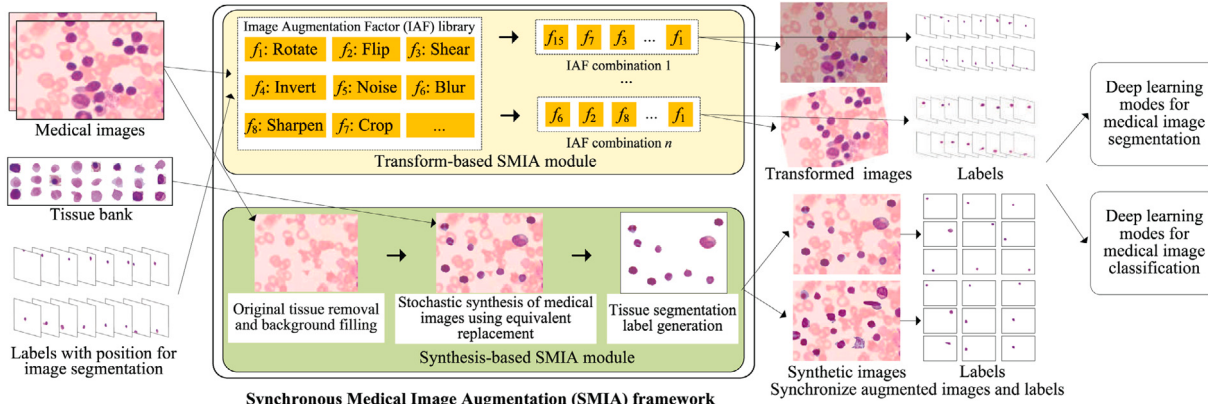


Fig. 2. Architecture of the proposed SMIA framework. The SMIA framework includes a transform-based SMIA module and a synthesis-based SMIA module. Both of them can generate category-balanced and diverse image-label pairs, and use them as training data for DL-based image segmentation tasks.

3. Synchronous medical image augmentation framework

In this section, we describe the architecture of the proposed Synchronous Medical Image Augmentation (SMIA) framework, as well as the theoretical basis operational factors of image augmentation. In Section 3.1, we introduce the framework pipeline and main components of the framework, including an Image Augmentation Factor (IAF) library, a transform-based SMIA module, and a synthesis-based SMIA module. In Section 3.2, we analyze the unique characteristics of medical images, which is the theoretical basis for constructing the image augmentation factor library. On this basis, in Section 3.3, we use atomic transformation operations to build an image augmentation factor library, and serve as an important component of the SMIA framework.

3.1. Overall architecture

As shown in Fig. 2, the proposed SMIA framework includes a transform-based SMIA module and a synthesis-based SMIA module. Given an original medical image set for image segmentation DL model training, we first annotate each image sample, extract the target segmentation objects (i.e., medical tissues or organs), and treated them as segmentation labels and ground truths. Through this step, we can obtain the images of all segmentation objects and the positions of the objects in the original image. The image set of the segmentation objects without position forms a tissue bank. In addition, each medical image and the segmentation object images with position information further constitute an image-label pair, which can be used as a sample

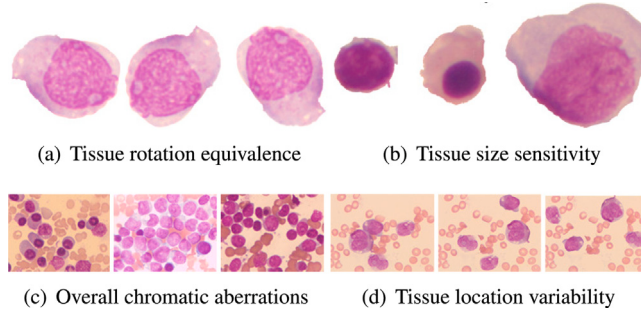


Fig. 3. Characteristics of medical images or tissues.

for image segmentation model training. It is worth noting that each medical image may contain one or more segmentation objects.

The original medical images, tissue bank, and corresponding labels are input into the SMIA framework for image augmentation. In the transform-based SMIA module, for each medical image sample and its tissue segments, a subset of SMIA factors with a random number of factors and stochastic parameter values are selected to simultaneously generate augmented samples and the paired tissue segments. In the synthesis-based SMIA module, we randomly replace the original tissues with the augmented tissues using an equivalent replacement method to synthesize new medical images, which can well maintain the original medical implications. In order to keep the same number and category of tissues as the original image, we randomly select the augmented tissues and insert them into the background-filled images to re-synthesize new medical images.

Both of the transform-based SMIA module and the synthesis-based SMIA module can generate category-balanced and diverse image-label pairs, and use them as training data for image segmentation DL models. In addition, it is not difficult to understand that the augmented medical images can also be used for the DL model training of medical image classification.

3.2. Theoretical basis of medical image augmentation

To provide an effective SMIA operation for medical images, we delve into the specific characteristics of medical images and tissues and provide a theoretical basis for medical image augmentation. Examples of specific characteristics of medical images and tissues are shown in Fig. 3.

(1) **Tissue rotation equivalence.** Many medical images and tissues have rotationally equivalent features, namely, the flipped/rotated image maintains the same medical implications as the original image. For example, a flipped or rotated BMS image retains the same blood structure and cell shape as the original image. In addition, due to the motility of leukocytes and red blood cells in the blood, they can be rotated or flipped in the BMS image, which does not change their medical implications, as shown in Fig. 3(a). Therefore, we can perform a rotation or flip operation on this type of medical images or tissues and generate new augmented images. Considering that not all medical images hold this characteristic, we need to check the rotational equivalence of each medical image dataset before image augmentation.

(2) **Tissue size sensitivity.** In the medical field, the size of a lesion or tissue usually has important medical implications. For example, when diagnosing leukemia by bone marrow smears, doctors typically identify abnormally growing leukocytes by observing their size, as shown in Fig. 3(b). Therefore, for medical images with tissue size sensitivity characteristics, we exclude the image scaling operation in the proposed SMIA framework.

(3) **Overall chromatic aberrations.** In color medical image processing applications, medical images between different acquisition batches may have overall chromatic aberrations due to factors such as

illumination, staining, and imaging equipment, as shown in Fig. 3(c). Traditional ML methods typically use color normalization techniques to adjust the overall chromatic aberration of all images. In contrast, most DL models prefer to use raw medical images to train the models without complex preprocessing. Therefore, we respect the inevitable phenomenon of overall chromatic aberrations and apply color adjustment operations to simulate the overall chromatic aberration of medical images.

(4) **Tissue position variability.** We note that changes in the position of lesions or tissues in some medical images do not affect medical implications. For example, in a BMS image, because of the movement of blood, the position of cells changes in different time periods, as shown in Fig. 3(d). For dermoscopic images, due to different photographing angles, the position of lesions in different images is not fixed. Hence, if the position of tissues changes without affecting its medical implications, we can define that the tissue has position variability. We can increase sample diversity by adjusting the position of the tissues during image augmentation. We need to check the tissue position variability of each medical image dataset before image augmentation.

3.3. Image augmentation factor library

Based on transformation operations of the IMGAUG project (Jung, 2017), we build an Image Augmentation Factor (IAF) library by collecting more than 24 transformation operations, each of which is called an augmentation factor. Examples of the augmentation results are shown in Fig. 4.

(1) Affine transformation factors.

Affine transformation is a traditional image processing method widely used for image augmentation, including rotation, flipping, tilting, translating, cropping, and piecewise affine. Considering that scaling operations may change the size of tissues, which conflicts with the specific characteristics of tissue size sensitivity, we exclude them from image augmentation factors.

(2) Color transformation factors.

Based on the overall chromatic aberration of medical images, we introduce several color transformation operations as augmentation factors, including super-pixel, color space change, gray scaling, invert, contrast normalization, and histogram equalization. We apply histogram equalization to each channel of a medical image. By transforming the histogram of the original medical image into uniform distribution, we increase the dynamic range of the gray value of all pixels, thus increasing the overall contrast of the image.

(3) Pixel overlay factors.

To promote the diversity of medical and tissue images, we introduce a set of pixel overlay operations as image augmentation factors, including pixel adding, pixel multiply, embossing, edge detection, and sharpen.

(4) Noise factors.

To generate medical images with noisy data and increase their diversity, we introduce different noise functions as image augmentation factors, such as Additive White Gaussian noise (AWGN), random noise, and dropout functions.

(5) Blur factors.

In this work, we use different blur functions as augmentation factors, such as Gaussian blur, median blur, motion blur, and bilateral blur.

4. Transform-based and synthesis-based SMIA modules

In this section, we describe the transform-based SMIA module and the synthesis-based SMIA module in detail. In Section 4.1, we introduce the main stages of the transform-based SMIA module, such as medical image and tissue preparation, stochastic IAF combination, and synchronous augmentation. In Section 4.2, we present the main steps of

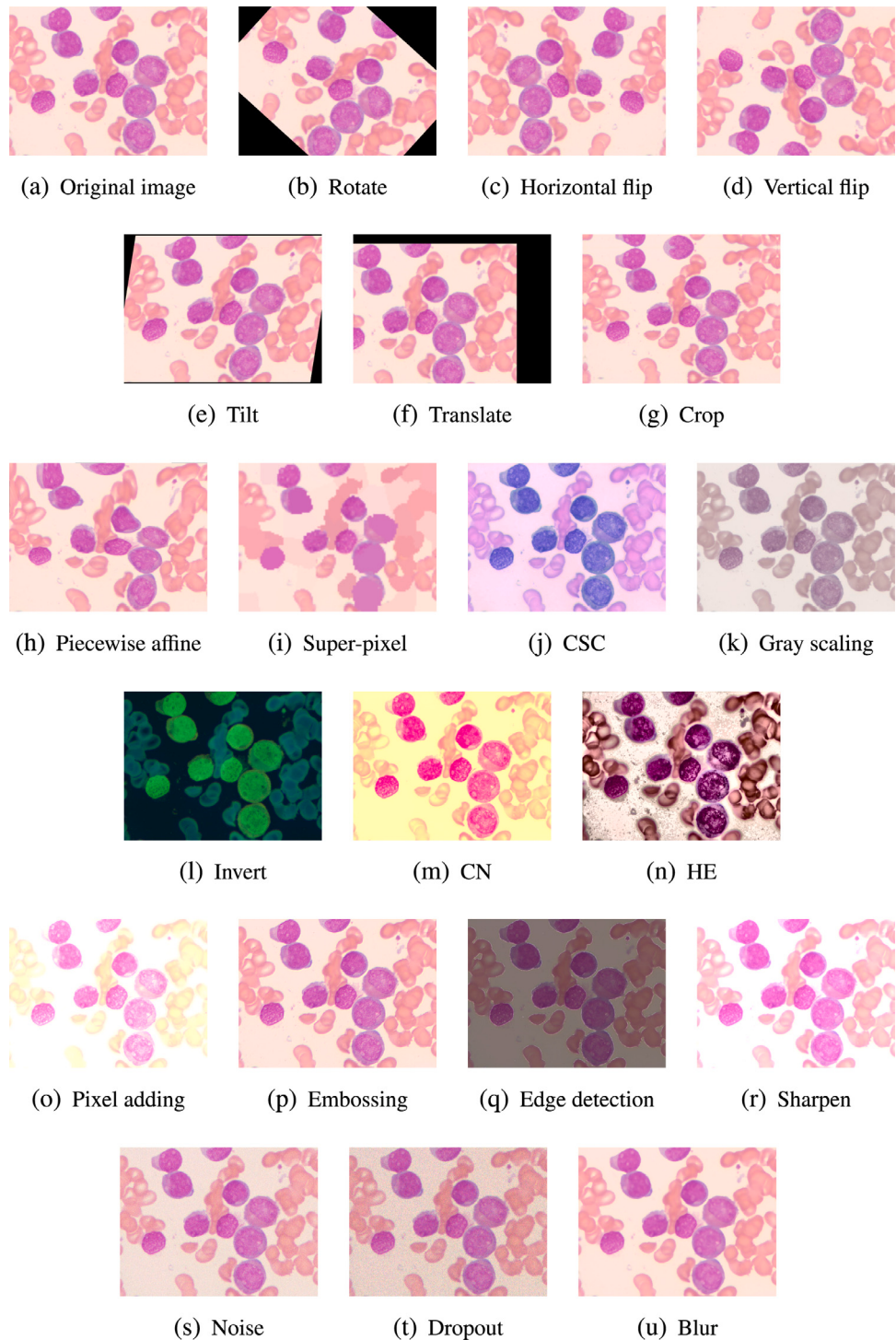


Fig. 4. Examples of the image augmentation factors. (j) CSC: Color Space Change, (m) CN: Contrast Normalization, (n) HE: Histogram Equalization.

the synthesis-based SMIA module, including tissue extraction and augmentation, medical image synthesis, and image-label pair generation. Both of two SMIA modules can provide large-scale and diverse training data for DL models of medical image segmentation, and improve the accuracy of the models.

4.1. Transform-based SMIA module

Based on the IAF library, we propose a transform-based SMIA module for medical images and the corresponding tissue segments (segmentation labels) to generate large-scale, diverse and annotated training

data for DL models of medical image segmentation. For each image sample and its segmentation labels, we perform the same stochastic IAF combination for them to generate different new samples and corresponding segmentation labels. In this way, augmented samples and labels also match each other, achieving the synchronous augmentation of the samples and their labels. The workflow of the transform-based SMIA module is shown in Fig. 5.

4.1.1. Medical image and tissue preparation

We gather a set of raw medical images as the original dataset for image augmentation. There may be one or more target tissues that need

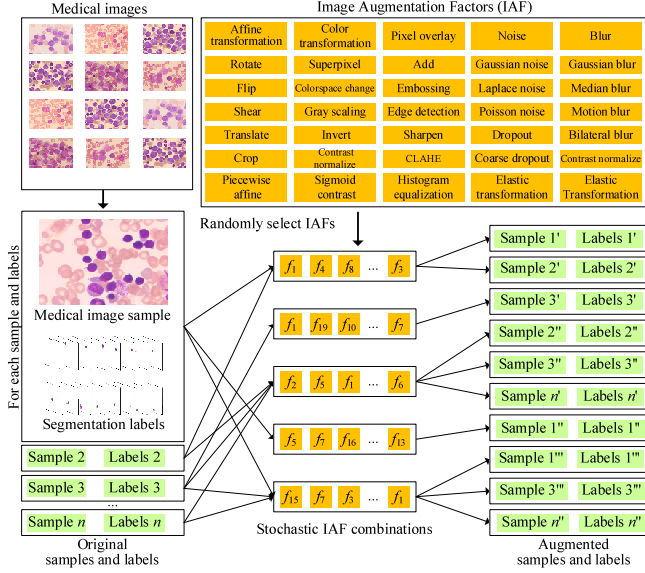


Fig. 5. Workflow of the transform-based SMIA module.

to be segmented and classified in each medical image. Provide a medical image, we extract each target tissue with its position information from the original image. We then create a new image with the same size as the original image and place the extracted tissue into the new image. In this way, the tissue in the new image is positioned the same as in the original image. That is, we generate a tissue image for each segmented tissue, in which there is only one tissue without background. In addition, we can easily get the corresponding ground truths of tissue from each tissue image, as shown in Fig. 1. For a medical image X_i , assuming that there are n_i target tissues, the corresponding tissue images $Y_i = \{y_{i,1}, \dots, y_{i,n_i}\}$ can be generated and treated as segmentation labels.

4.1.2. Stochastic IAF combination

To improve the diversity of medical images in the transformation process, we randomly select any number of IAFs from the IAF library to form a stochastic IAF combination. Let $IAFs = \{f_1, \dots, f_m\}$ be the IAF library with m IAFs, we select an IAF combination $IAFc_1$ with a random number of image augmentation factors and then initialize random values to the parameters of each factor. Repeat this step K times to generate K stochastic IAF combinations. In this way, no matter how many IAF combinations are generated, it will not lead to similarities between the transformation results, thus ensuring the diversity of the image samples.

4.1.3. Synchronous augmentation

Let $(X, Y) = \{(X_1, Y_1), \dots, (X_i, Y_i), \dots, (X_N, Y_N)\}$ be a set of medical images and tissue images, where X_i is a medical image sample, $Y_i = \{y_{i,1}, \dots, y_{i,n_i}\}$ is the tissue segmentation labels of X_i , and n_i is the number of target tissues of X_i . We generate a set of stochastic IAF combinations $IAFc = \{IAFc_1, \dots, IAFc_j, \dots, IAFc_K\}$. For each pair of sample and tissue segmentation labels (X_i, Y_i) . We use each IAF combination $IAFc_j \in IAFc$ to perform transformation operations on X_i and generate a new augmented sample X'_i . At the same time, we also use $IAFc_j$ to perform the same transformation operations on each tissue segment $y_{i,n_i} \in Y_i$ and generate the corresponding augmented label y'_{i,n_i} . In this way, $Y'_i = \{y'_{i,1}, \dots, y'_{i,n_i}\}$ and X'_i matches each other, achieving synchronous augmentation. In this way, we can select more IAF combinations on each medical image to generate more augmented images.

Definition 1 (Synchronous Augmentation). Synchronous augmentation means when we perform augmentation operations such as transformation or synthesis on samples (medical images/tissue images), we also generate the corresponding segmentation labels and classification labels that match the augmented samples.

Both of transform-based on synthesis-based SMIA methods provide synchronous augmentation. Two examples of synchronous augmentation are illustrated in Fig. 6. As shown in Fig. 6(a), in the transform-based SMIA method, given a tissue image with position information, we perform a rotation operation on it and get an augmented tissue image. At the same time, we need to perform the same operation on the segmentation label (ground truths) of the original tissue to synchronously generate an segmentation label that matches the augmented tissue image. We will explain Fig. 6(b) when we introduce the equivalent replacement.

As described above, many medical images from clinical and biomedical experimental applications are uneven in the number of samples between healthy and diseased samples or between different diseases. Unbalanced medical images will lead to bias in ML or DL results. To narrow the imbalance of samples in each category, we calculate the number of samples in each category and then propose a category-balanced strategy. We perform more transform operations on the samples of small categories so that the number of samples in each category is the same after the transformation. The detailed steps of the transform-based SMIA module are described in Algorithm 4.1.

Algorithm 4.1 Transform-based SMIA module

Input:

(X, Y) : the original medical images and tissue images;
 $IAFs$: the image augmentation factor library;

Output:

(X', Y') : the transformed medical images and tissue images.

```

1: generate stochastic IAF combinations  $IAFc = \{IAFc_1, \dots, IAFc_K\} \leftarrow IAFs$ ;
2: for each  $(X_i, Y_i)$  in  $(X, Y)$  do
3:   calculate the number  $k_i$  of transform operation according to the
      category-balanced strategy;
4:   randomly select  $k_i$  IAF combinations from  $IAFc$ ;
5:   for  $j$  from 1 to  $k_i$  do
6:     perform the transform operation on medical image  $X'_i \leftarrow IAFc_j(X_i)$ ;
7:     for each tissue image  $y_{i,n_i}$  in  $Y_i$  do
8:       perform the transform operation on  $y'_{i,n_i} \leftarrow IAFc_j(y_{i,n_i})$ ;
9:     generate a pair of transformed medical images  $(X'_i, Y'_i)$ ;
10:    append to the list  $(X', Y') \leftarrow (X'_i, Y'_i)$ 
11: return  $(X', Y')$ .
```

In Algorithm 4.1, assuming that the number of medical image samples X is N , the total number of all tissues in X is $M = \sum_{i=1}^N n_i$, and the total number of IAF combinations used in the transformation process is $K = \sum_{i=1}^N k_i$. Hence, the computational complexity of Algorithm 4.1 is $O(K(N + M))$.

4.2. Synthesis-based SMIA module

To further generate large-scale medical images and improve the diversity of training samples, we propose a synthesis-based SMIA module, which consists of two steps: (a) tissue extraction and augmentation, and (b) medical image synthesis. In the step of tissue extraction and augmentation, we extract the target tissues from each medical image and transform them to generate an augmented tissue database. In the step of medical image synthesis, tissues in a medical image are randomly replaced by the augmented ones to synthesize a new medical image. Finally, the corresponding segmentation labels of the synthesized image are simultaneously generated.

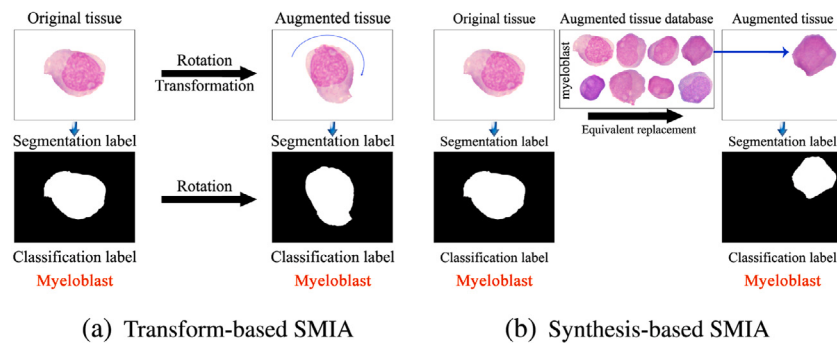


Fig. 6. Examples of synchronous augmentation.

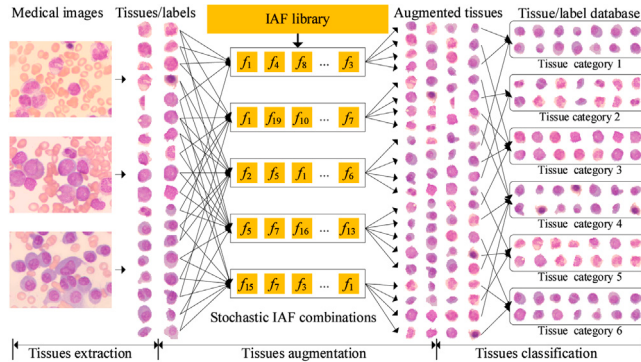


Fig. 7. Workflow of tissue extraction and augmentation

4.2.1. Tissue extraction and augmentation

To guarantee the diversity of synthetic medical images, we need to provide sufficiently diverse tissues. We extract all target tissues from the raw medical images and augment them using the transform-based SMIA module. Augmented tissues are classified and grouped into different categories to generate an augmented tissue database. The workflow of tissue extraction and augmentation is illustrated in Fig. 7.

(1) Tissue extraction.

We manually segment and extract all target tissues from each raw medical image, e.g., extract leukocytes from bone marrow smears and lesions from dermoscopic images. We then annotate and classify these tissues, so that each tissue has its own unique label (tissue name or category).

(2) Tissue augmentation.

We use the transform-based SMIA module to perform transformations on the extracted tissue images. We select random numbers of the stochastic IAF combinations to perform augmentation on each tissue image and generate large-scale and diverse augmented tissue images. Based on stochastic transformation, no matter how many tissues are augmented, it does not lead to similarities between them. Thereby ensuring the diversity of tissues in the augmentation process.

(3) Tissue classification.

Because the tissue augmentation process does not change the medical implications of each tissue, so the label or category of the tissue is maintained. Hence, augmented tissues are automatically labeled and classified using the labels of the original tissues. Finally, the original and augmented tissues are combined to form a tissue database, where the tissues of each category are grouped into corresponding subsets.

4.2.2. Medical image synthesis

In this process, we synthesize new medical images using original images and the augmented tissue databases. Target tissues in the original medical images are randomly replaced by the augmented tissues.

to synthesize new medical images, as well as generate the corresponding segmentation labels. The medical image synthesis process mainly includes three steps, including (a) original tissue removal and background filling, (b) stochastic synthesis of medical images, and (c) tissue segmentation label generation. The workflow of the medical image synthesis process is illustrated in Fig. 8.

(1) Original tissue removal and background filling.

Given a set of original medical images and corresponding target tissue images, we can manually and accurately identify the regions of all target tissues in each medical image. We remove all target tissues from each medical image and fill the hollowed-out areas with the background color. Considering the overall chromatic aberrations of the medical images, we cannot use a fixed value as the background color of different images. We use the image restoration method proposed by Telea (Telea, 2004) for background filling, where the filling process starts from the boundary of the hollowed-out area and gradually enters the area. Each filling pixel is replaced by a weighted amount of all pixels in the neighborhoods.

(2) Stochastic synthesis of medical images using equivalent replacement.

For each medical image, we can get the categories of the original tissues and the size of each category based on the tissue classification labels. Let X_i be a medical image that contains a collection of tissues $Y_i = \{y_{i,1}, \dots, y_{i,n_i}\}$, it is assumed that these tissues can be divided into c_i categories. We get the categories of Y_i and the number of tissues in each category. For each category, we randomly select the same number of tissues from the augmented tissue database Y' using a reverse way. In this approach, we can select the augmented tissues for all categories of Y_i to form a set of candidate tissues Y'_i . As described above, this work focuses on medical images with tissue location variability. For example, the position of leukocytes and red blood cells in BMS images has no impact on disease features. Hence, we place the selected tissues at arbitrary and non-conflicting positions in the background-filled medical image to generate a new synthetic medical image.

Definition 2 (Equivalent Replacement). Equivalent replacement means for each original tissue in a medical, we randomly select an augmented tissue from the same category of the augmentation tissue bank and replace the original tissue. Although the original tissue is removed, the same medical characteristics are maintained because the replaced tissue belonged to the same category.

An example of equivalent replacement is given in Fig. 9(b). Given a medical image, if there is only one original tissue, we can randomly select one tissue from the augmented tissue database with the same category. We then place the selected tissue at an arbitrary position in the background-filled image to generate a new synthetic medical image. Otherwise, we need to consider the category of the original tissues and replace the same number and category of augmented tissues to generate a new synthetic image. Based on the equivalent replacement method, the synthetic image keeps the same number and category of

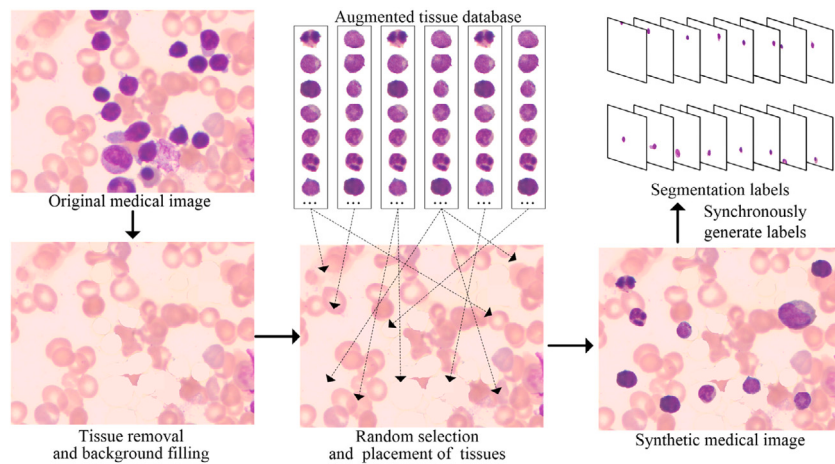


Fig. 8. Workflow of the medical image synthesis process.

tissues as the original image. Since the number and category between the augmented tissues and the original tissues are the same, it is easy to prove that each synthetic medical image has a medical meaning similar to the original image. Therefore, we put each new synthetic image into the medical category in which the original image is located.

4.2.3. Image-label pair generation

After synthesizing a new medical image, we generate corresponding tissue segmentation labels based on the augmented tissues and position information. For each tissue in the current synthetic image, we create a new image with the same size and then place the tissue in the new image with the same position. That is, we generate a tissue image for each tissue and term as a segmentation label.

To provide a category balanced training data, we perform more synthesis operations on small-categories samples, so that the number of samples in each category is the same after synthesis. The detailed steps of the synthesis-base SMIA module are detailed in module 4.2.

Assuming that the number of X is N , the total number of all tissues in X is $M = \sum_{i=1}^N n_i$, and the total number of IAF combinations used in the synthesis process is $K = \sum_{i=1}^N k_i$. The computation complexity of the process of tissue augmentation is $O(M)$, that of the process of background filling is $O(N)$, and that of the process of medical image synthesis is $O(NK)$. Hence, the computational complexity of Algorithm 4.2 is $O(M + N + NK)$.

5. Experiments

In this section, we conduct extensive experiments to evaluate the effectiveness of the proposed SMIA framework. In Section 5.1, we describe the experimental setup and the datasets used in the experiments. In Section 5.2, we discuss the experimental results of the transform-based SMIA module and the synthesis-based SMIA module. In Section 5.3, we further compare the proposed SMIA framework with the related medical image augmentation methods in terms of effectiveness, accuracy, and performance. In Section 5.4, we introduce DL models for image segmentation and classification on bone marrow smear and dermoscopic images to demonstrate that our algorithms have a positive impact on the performance of these models.

5.1. Experimental setting

We implement the proposed transform-based and synthesis-based SMIA modules and perform a series of experiments to evaluate the effects and performance. The proposed SMIA framework is implemented

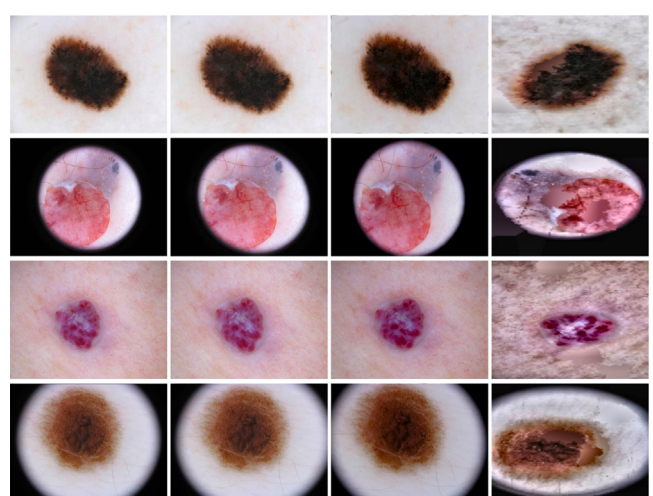
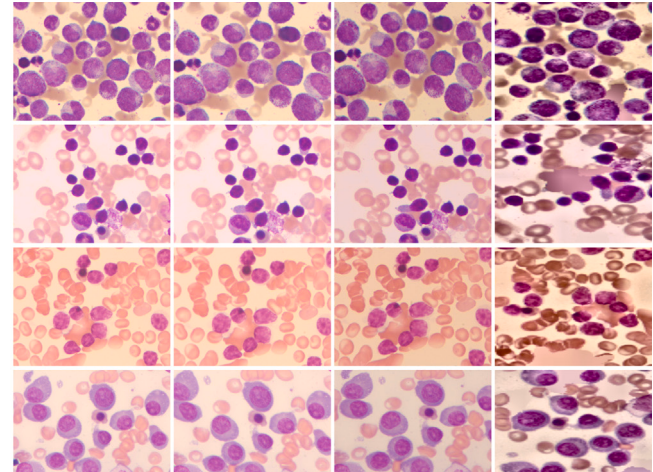


Fig. 9. Augmentation results of the transform-based SMIA module.

Algorithm 4.2 Synthesis-based SMIA module**Input:**

(X, Y) : the original medical images and tissue images;

$IAFs$: the image augmentation factor library;

Output:

(X'', Y'') : the synthetic medical images and tissue images.

```

1: // Transform tissues and build a tissue database (tissue augmentation).
2: generate stochastic IAF combinations  $IAFc = \{IAFc_1, \dots, IAFc_K\} \leftarrow IAFs$ ;
3: for each set of tissue images  $Y_i$  in  $Y$  do
4:   perform the transform operation on tissue images  $Y'_i \leftarrow IAFc(Y_i)$ ;
5:   append to the augmented tissue database  $Y' \leftarrow Y'_i$ ;
6: // Remove original tissues and fill background of medical images
   (background filling).
7: for each medical image  $X_i$  in  $X$  do
8:   remove all target tissues from  $X_i$ ;
9:   fill background  $X_i(g) \leftarrow X_i$ ;
10: // Stochastic selection and placement of augmented tissues
    (medical image synthesis).
11: for each background filled image  $X_i(g)$  in  $X(g)$  do
12:   calculate the number  $k_i$  of synthesis operation according to the
      category-balanced strategy;
13:   get the categories of  $Y_i$  and the number of tissues in each
      category;
14:   for  $j$  from 1 to  $k_i$  do
15:     randomly select the same categories and the same number of
      augmented tissues  $Y''_i$  from  $Y'$ ;
16:     place  $Y''_i$  at any non-conflicting position in  $X_i(g)$ ;
17:     synthesize new medical image  $X''_i$  and generate segmentation
      labels  $Y''_i$ ;
18:     append to the list  $(X'', Y'') \leftarrow (X''_i, Y''_i)$ ;
19: return  $(X'', Y'')$ .

```

Table 1

Medical image data used in the experiments.

Dataset name	Original/augmented	#No. sample	#No. labels
BMS dataset	Original images	250	3400
BMS dataset	Augmented images	70,000	1,190,000
Dermoscopic dataset	Original images	500	500
Dermoscopic dataset	Augmented images	70,000	70,000

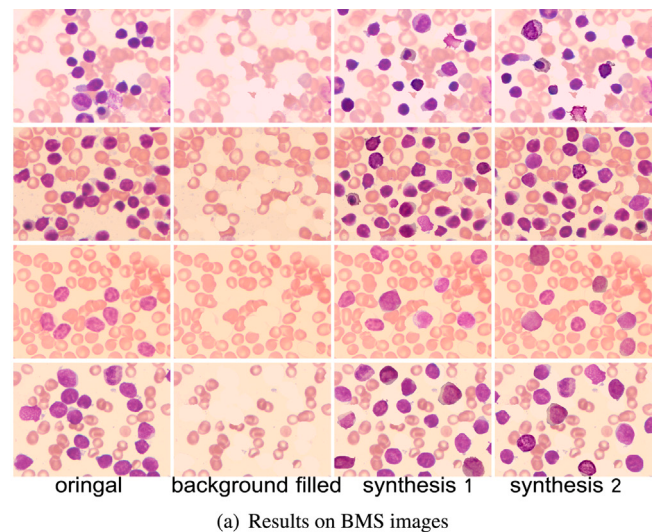
in python 3.5. Two groups of medical image data are used in the experiments, including BMS images from our hospital and dermoscopic images from the International Skin Imaging Collaboration (ISIC) public database (Archive, 2017). The data description of the used medical images is shown in Table 1.

In the case of the BMS image dataset, we collect 250 BMS images from an actual clinical project as original samples, which contain 12 blood diseases, such as acute myeloid leukemia, acute lymphocytic leukemia, chronic lymphocytic leukemia, chronic myeloid leukemia, multiple myeloma, and plasma cell leukemia. Each BMS image usually contains multiple leukocytes and red blood cells. We manually extract 3400 leukocytes from these images as target tissue segments, and the extracted cells contain 22 categories of leukocytes. In the case of the dermoscopic image dataset, we select 500 dermoscopic images from ISIC, including 12 skin diseases. Each dermoscopic image usually contains a lesion, such as melanoma, nevus, angioma, basal cell carcinoma, lentigo, and scar.

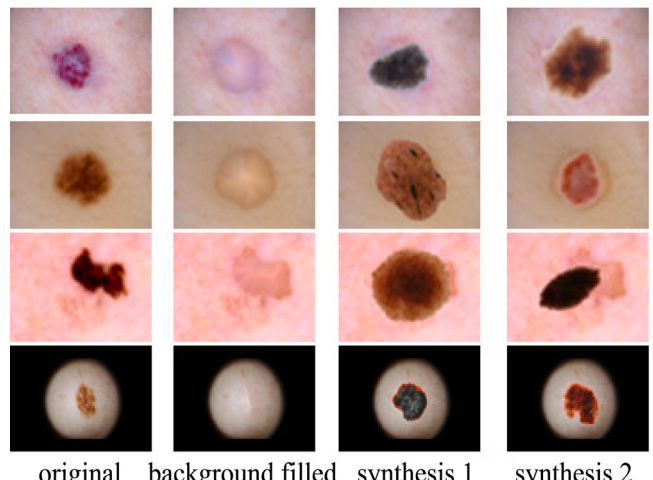
5.2. Image augmentation results

5.2.1. Results of transform-based SMIA module

We perform the transform-based SMIA module on the MBS and dermoscopic images and observe the augmentation results by using



(a) Results on BMS images



(b) Results on dermoscopic images

Fig. 10. Augmentation results of the synthesis-based SMIA module.

different numbers of stochastic IAF combinations. In the experiments, we respectively use three groups of stochastic IAF combinations with different numbers of IAFs on each MBS image and dermoscopic image. We select 4 groups of BMS and dermoscopic images to observe the augmentation results. Augmentation results of the transform-based SMIA module on these medical images are shown in Fig. 9.

As can be seen from Fig. 9, since the stochastic image augmentation factors are used, the augmentation results of each image are different from each other. In Case (1), we randomly use three IAFs on each original image, such as contrast normalization, sharpen, and perspective affine. In Case (2), we superimpose 3 other IAFs on the basis of Case (1), including Gaussian blur, pixel adding, and elastic transformation. In Case (3), we superimpose 3 other IAFs on the basis of Case (2), including superpixels, rotate, and histogram equalization. It is clearly observed that as the number of IAFs increases, the difference between the augmented images and the original images increases. The proposed transformed SMIA module can promote the diversity of medical images.

5.2.2. Results of synthesis-based SMIA module

We perform the synthesis-based SMIA module with 250 original BMS images and 500 original dermoscopic images to randomly generate 7000 synthetic images, respectively. We select 4 groups of BMS and dermoscopic images to observe the synthesis results. Each group

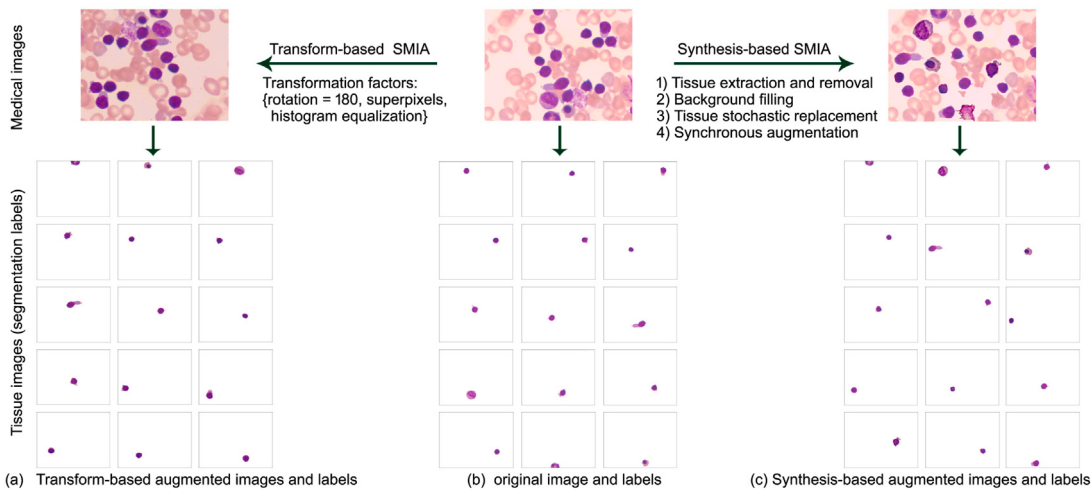


Fig. 11. Synchronous augmentation results of the SMIA framework on a bone marrow smear image and its segmentation labels. **Fig. 11(b)** shows the original medical image (bone marrow smear) and the corresponding leukocyte images (segmentation labels). We perform transform-based augmentation on these images to obtain **Fig. 11(a)**, and perform synthesis-based augmentation to obtain **Fig. 11(c)**. Specifically, for the original medical image and each leukocyte image, we use the same transformation factors to perform the transform-based SMIA operation, so as to obtain the augmented medical image and the matched labels. For **Fig. 11(c)**, firstly extract all leukocyte tissues in the original image and remove them from the image, and then fill the blank area to get a background image without leukocyte tissues. Then, according to the invariable nature of cell flow, the extracted leukocyte tissues are placed in the random positions of the background image to form a new augmented image. At the same time, the matching augmented labels are synchronously generated according to the placement position of each tissue.

contains one original image and three synthetic images. Augmentation results of the synthesis-based SMIA module on these medical images are shown in **Fig. 10**.

As can be observed in **Fig. 10**, in each synthetic image, the augmented tissues can be seamlessly inserted into the medical image, maintaining the same number and category of tissues as the original image. From the background-filled images, we can note that the target tissues are completely removed from each image and the hollowed-out areas are seamlessly filled with surrounding background pixels. In addition, selected augmented tissues of each category are randomly selected and inserted into random positions in the synthetic image. The augmentation results show that the synthesis-based SMIA module can generate large-scale diverse augmented medical images with medical implications.

5.2.3. Evaluation of synchronous augmentation

We further evaluate the synchronization effects of the proposed transform-based and synthesis-based SMIA module by observing the augmented medical image samples and their segmentation labels. We selected a BMS image with 16 leukocytes and respectively perform the transform-based and synthesis-based SMIA modules on it and its tissue images. The synchronization effects of the SMIA modules are shown in **Fig. 11**.

We can observe from **Fig. 11(b)** that since the original BMS sample and its tissue segments use the same IAF combination, the transformed sample matches the transformed tissues (segmentation labels), achieving synchronous augmentation. In **Fig. 11(c)**, the synthesized BMS sample and its segmentation labels also achieve synchronous augmentation. Therefore, experimental results demonstrate that both the transform-based SMIA and synthesis-based SMIA modules can provide synchronous augmentation and automatically generate the ground truths of tissue segments.

5.3. Performance comparison

We conduct experiments to evaluate the performance of the proposed SMIA modules in terms of transformation and synthesis operations. All performance experiments are conducted in a high-performance computer equipped with Intel Core i7-10750H 6-core CPU, 16 GB DRAM, 1TB SSD, and NVIDIA Quadro P620.

5.3.1. Execution time evaluation

We select four groups of MBS images with different numbers of leukocytes. The average number of leukocytes in each image of the four groups is 5, 10, 15, and 20, respectively. For each group, we respectively perform the transform-based and synthesis-based SMIA operations to generate augmented samples of different scales and corresponding segmentation labels. We record the execution time of each case, and the evaluation results are presented in **Fig. 12**.

Fig. 12(a) shows the execution time of the transform-based SMIA module on different scales of BMS images. Obviously, the more leukocytes in each BMS image, the more transformation time we need. When each image contains 5 leukocytes, we generate 4000 samples and corresponding 20,000 leukocyte images using 557 mins. When each image contains 20 leukocytes, we generate 4000 samples and corresponding 80,000 leukocyte images using 1739 mins. Experimental results indicate the efficiency of the transform-based SMIA module. We can obtain large-scale transformed BMS images and synchronous segmentation labels in an acceptable time.

Fig. 12(b) shows the execution time of the synthesis-based SMIA operation. Compared to the transform-based method, the average execution time of the synthesis-based method is significantly reduced. For example, in the case of 8000 staples with 16,000 leukocytes, we use 2957 mins for the transformation operation and only 287 mins for the synthesis operation. That is because we do not need to transform and augment tissues for each BMS image transformation process, just select them from the augmented tissue database. In addition, since it is only necessary to insert tissues into the synthetic images without separately transforming each tissue, the number of tissues in each image has a small influence on the execution time of the synthesis operation. For example, to synthesize 4000 BMS images, synthesis operations on 5 leukocytes cost 86 mins, 118 mins on 10 leukocytes, and 216 mins on 20 leukocytes. Experimental results show that both the transform-based and synthesis-based SMIA modules can efficiently provide image augmentation on medical images and tissues. Furthermore, the synthesis-based SMIA module significantly outperforms the transform-based SMIA module.

5.3.2. Accuracy comparison

We further evaluate the effectiveness of the proposed SMIA framework by introducing two existing medical image augmentation methods

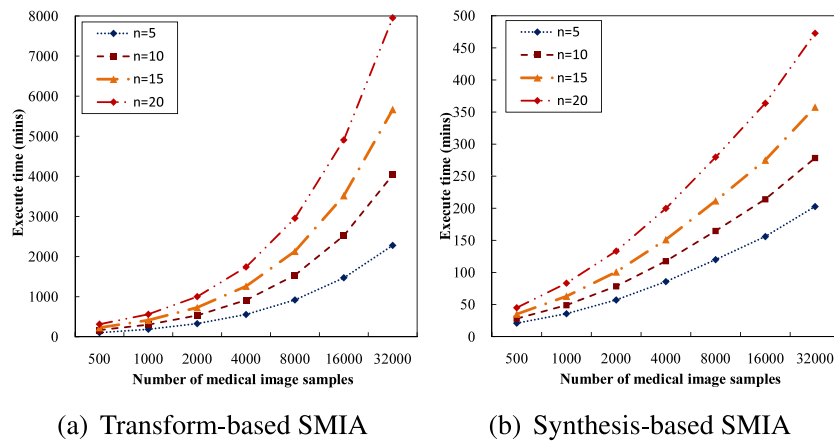


Fig. 12. Performance evaluation of the SMIA module.

Table 2

Augmentation effectiveness of the proposed SMIA modules and relevant methods. Dice similarity coefficient (DICE), the average symmetrical surface distance (ASD), the 95th percentile of the Hausdorff distance (HD95) are used as evaluation criteria.

Methods	DSC (%)	ASD (mm)	HD95 (mm)
Transform-based SMIA	89.75	3.35	4.77
Synthesis-based SMIA	90.67	3.81	4.92
Multiple-snapshot (Zaman et al., 2020)	86.36	4.24	12.25
WGAN-GP-SN (Kossen et al., 2021)	84.73	6.57	15.90

in the comparison experiments, including a multiple-snapshot algorithm (Zaman et al., 2020) and a WGAN-GP-SN algorithm (Kossen et al., 2021). All comparative experiments are conducted under the same hardware environment and the same BMS image set was used. Three evaluation criteria, such as the Dice similarity coefficient (DICE), the average symmetrical surface distance (ASD), the 95th percentile of the Hausdorff distance (HD95) are used to evaluate the effectiveness of the comparison methods.

DSC (Dice, 1945) is a collective similarity measure used to calculate the similarity of two samples.

$$DSC = \frac{2TP}{FP + 2TP + FN}, \quad (1)$$

where TP is true positive, FP is false positive, and FN is false negative. DSC values range from 0 to 1. The best value of the result is 1 and the worst value is 0. ASD constrains the matching rate of augmented volume surface boundary. Assuming that S_a and S_b represent the augmented result and ground truth, respectively, then ASD is defined as:

$$ASD = \frac{\sum_{a \in S_a} d(a, S_b) + \sum_{b \in S_b} d(b, S_a)}{|S_a| + |S_b|}, \quad (2)$$

where a and b is a pixel in S_a and S_b , respectively. The unit of ASD is mm. Hausdorff distance is a measure describing the degree of similarity between two images. 95th-percentile Hausdorff distance (HD95) between S_a and S_b is defined as:

$$HD95 = \max(h(S_a, S_b), h(S_b, S_a)), \\ h(S_a, S_b) = \max_{a \in S_a} \left\{ \min_{b \in S_b} \|a - b\| \right\}, \quad (3)$$

where $\|\cdot\|$ is the distance normal form between S_a and S_b . The comparison results of the proposed SMIA modules and relevant methods are shown in Table 2.

We compare the tissues in the augmented image with the tissues in the augmented segmentation labels to calculate the values of the three evaluation indicators. It can be seen from Table 2 that the two SMIA modules designed in this paper can obtain more accurate augmentation results than the other two comparative methods. For

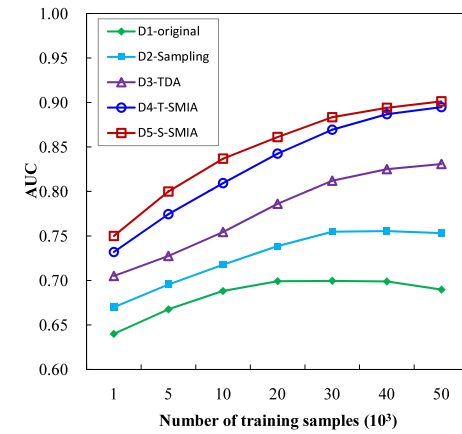


Fig. 13. Performance comparison of SegNet image segmentation DL model.

example, the DSE values of the transform-based SMIA and synthesis-based SMIA modules are similar, about 90%. In contrast, the ASD and HD95 values of the multiple-snapshot and WGAN-GP-SN methods are higher than our modules. Although WGAN-GP-SN uses deep learning technique, it is mainly used to generate diverse image samples, but it is difficult to synchronously generate segmentation labels that are highly matched with the image samples. That is to say, the medical image generated by our SMIA framework has a higher matching degree with the segmented label, thus obtaining a high-quality training data set for DL-based medical image segmentation tasks.

5.4. Impact on image segmentation and classification

We evaluate the impact of augmented training data on the performance of DL models for medical image segmentation and classification. We generate five groups of augmented medical image data by using different augmentation methods, as shown in Table 3.

5.4.1. Impact on image segmentation DL model

We use the SegNet (Badrinarayanan et al., 2017) model as an image segmentation model to evaluate the impact of the augmented data on the performance of the model. The SegNet model is trained using the five data in Table 3 with different data sizes. We use an independent testing set to compare the performance of each model by using the area under the ROC curve (AUC). The performance comparison results of the SegNet image segmentation model are shown in Fig. 13.

As can be seen from Fig. 13, the SegNet model trained by D4-T-SMIA and D5-S-SMIA data generated by the SMIA modules obtains

Table 3
Augmented training sets using different methods.

Training set	Descriptions
D1-original	Training dataset using the original medical images.
D2-sampling	Training dataset augmented by upsampling and downsampling method.
D3-TDA	Training dataset augmented by traditional geometric transformation method.
D4-T-SMIA	Training dataset augmented by the transform-based SMIA module.
D5-S-SMIA	Training dataset augmented by the synthesis-based SMIA module.

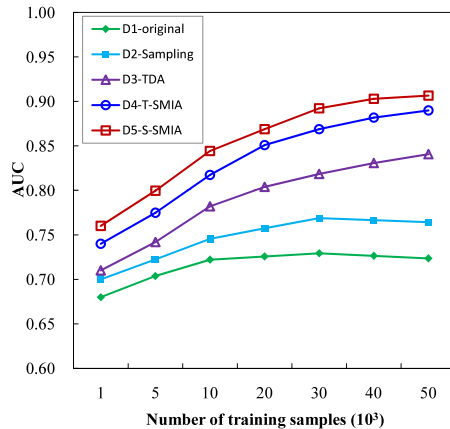


Fig. 14. Performance comparison of CNN image classification models.

better AUC values than the models trained based on D1-original, D2-sampling, and D3-TDA datasets. When the number of training samples exceeds 40,000, the performance of the models based on D1-original and D2-sampling is degraded by over-fitting. Using the traditional augmentation method, D3-TDA marginally improves the accuracy of the SegNet models. In contrast, D4-T-SMIA and D5-S-SMIA generated by the transform-based and synthetic-based SMIA modules make the performance of the SegNet models significantly higher than the former three cases. Furthermore, benefitting from the stochastic augmentation strategy, the proposed SMIA framework increase the diversity of training samples. As the number of training samples increases, the performance of the SegNet models continues to increase.

5.4.2. Impact on image classification DL model

To further evaluate the impact of the augmented data on the performance of image classification DL models, we use the CNN model to participate in the experiments. We also use the AUC to evaluate the testing performance of the CNN model in each case. The performance comparison results of the CNN image classification model are shown in Fig. 14.

As shown in Fig. 14, the CNN model trained on the augmented images of D4-T-SMIA and D5-S-SMIA obtains higher AUC values than the models trained on D1-original, D2-sampling, and D3-TDA sets. For example, the CNN model obtains average AUC values of 0.85 and 0.83 on D4-T-SMIA and D5-S-SMIA datasets, while achieving average AUC values of 0.72, 0.75, and 0.79 on D3-TDA, D2-sampling, and D1-original, respectively. In addition, as the number of training samples increases, in most cases, the AUC value of CNN models trained by D3-TDA, D4-T-SMIA, and D5-S-SMIA increases. However, similar to image segmentation experiments, the original and sampling-based datasets also lead to over-fitting problems. The experimental results show that the proposed SMIA framework can provide large-scale, diverse medical image training data, and significantly improve the performance of image classification DL models.

6. Conclusion

This paper presented two Synchronous Medical Image Augmentation (SMIA) modules based on stochastic transformation and synthesis.

We built a SMIA library by collecting a series of atomic transformation operations. The transform-based SMIA module performs stochastic transformation operations on each medical image and its tissue images to simultaneously generate augmented samples and paired segmentation labels. In the synthesis-based SMIA module, medical tissues are extracted, augmented, and stochastically replaced into the background-filled images to re-synthesize new medical images. The proposed SMIA modules can well achieve synchronous augmentation between samples and corresponding tissue segmentation labels, and keep the diversity between different samples and different augmentation processes. Benefiting from stochastic transformation and synthesis augmentations, we can generate large-scale category-balanced, diverse and annotated training data. Extensive experimental results demonstrate that the proposed SMIA framework can significantly improve the performance of DL models for medical image segmentation and classification.

For future work, we will continue to explore the characteristics of different types of medical images and propose more data medical image augmentation methods.

CRediT authorship contribution statement

Jianguo Chen: Method design, Writing. **Nan Yang:** Data analysis. **Yuhui Pan:** Method design. **Hailing Liu:** Conduct experiments, Validation. **Zhaolei Zhang:** Writing – review & editing.

Declaration of competing interest

The authors declare that they have no known competing financial interests or personal relationships that could have appeared to influence the work reported in this paper.

Acknowledgments

This work is partially funded by the National Natural Science Foundation of China under Grant No. 62002110 and the International Postdoctoral Exchange Fellowship Program under Grant No. 20180024.

References

- Archive, I., 2017. ISIC: The International Skin Imaging Collaboration. Website, <https://isic-archive.com>.
- Badrinarayanan, V., Kendall, A., Cipolla, R., 2017. SegNet: A deep convolutional encoder-decoder architecture for image segmentation. *IEEE Trans. Pattern Anal. Mach. Intell.* 39 (12), 2481–2495.
- Cao, B., Wang, N., Li, J., Gao, X., 2018. Data augmentation-based joint learning for heterogeneous face recognition. *IEEE Trans. Neural Netw. Learn. Syst.* 99 (1), 1–13.
- Chaitanya, K., Karani, N., Baumgartner, C.F., Erdil, E., Becker, A., Donati, O., Konukoglu, E., 2021. Semi-supervised task-driven data augmentation for medical image segmentation. *Med. Image Anal.* 68, 101934.
- Chen, S., Gao, D., Wang, L., Zhang, Y., 2020. Cervical cancer single cell image data augmentation using residual condition generative adversarial networks. In: 2020 3rd International Conference on Artificial Intelligence and Big Data (ICAIBD). pp. 237–241.
- Chen, L.-C., Papandreou, G., Schroff, F., Adam, H., 2017. Rethinking atrous convolution for semantic image segmentation. *ArXiv E-Prints*.
- Chen, Y., Yang, X.-H., Wei, Z., Heidari, A.A., Zheng, N., Li, Z., Chen, H., Hu, H., Zhou, Q., Guan, Q., 2022. Generative adversarial networks in medical image augmentation: A review. *Comput. Biol. Med.* 144, 105382.
- Chlap, P., Min, H., Vandenberg, N., Dowling, J., Holloway, L., Haworth, A., 2021. A review of medical image data augmentation techniques for deep learning applications. *J. Med. Imaging Radiat. Oncol.* 65, 545–563.

- Dice, L.R., 1945. Measures of the amount of ecologic association between species. *Ecology* 26 (3), 297–302.
- Frid-Adar, M., Diamant, I., Klang, E., Amitai, M., Greenspan, H., 2018a. GAN-based synthetic medical image augmentation for increased CNN performance in liver lesion classification. *Neurocomputing* 321, 321–331.
- Frid-Adar, M., Klang, E., Amitai, M., Goldberger, J., Greenspan, H., 2018b. Synthetic data augmentation using GAN for improved liver lesion classification. In: International Symposium on Biomedical Imaging (ISBI). IEEE, pp. 289–293.
- Guan, Q., Chen, Y., Wei, Z., Heidari, A.A., Hu, H., Yang, X.-H., Zheng, J., Zhou, Q., Chen, H., Chen, F., 2022. Medical image augmentation for lesion detection using a texture-constrained multichannel progressive GAN. *Comput. Biol. Med.* 145, 105444.
- He, Y., Wang, A., Li, S., Yang, Y., Hao, A., 2022. Nonfinite-modality data augmentation for brain image registration. *Comput. Biol. Med.* 147, 105780.
- He, K., Zhang, X., Ren, S., Sun, J., 2016. Deep residual learning for image recognition. In: The IEEE Conference on Computer Vision and Pattern Recognition (CVPR). IEEE, pp. 770–778.
- Jung, A., 2017. imgaug. Website, <https://imgaug.readthedocs.io>.
- Kosken, T., Subramiam, P., Madai, V.I., Hennemuth, A., Hildebrand, K., Hilbert, A., Sobesky, J., Livne, M., Galinovic, I., Khalil, A.A., Fiebach, J.B., Frey, D., 2021. Synthesizing anonymized and labeled TOF-MRA patches for brain vessel segmentation using generative adversarial networks. *Comput. Biol. Med.* 131, 104254.
- Lin, G., Milan, A., Shen, C., Reid, I., 2017. RefineNet: Multi-path refinement networks for high-resolution semantic segmentation. In: The IEEE Conference on Computer Vision and Pattern Recognition (CVPR). IEEE, pp. 1925–1934.
- Rahim, T., Novamizanti, L., Nyoman, I., Shin, S.Y., 2021. Compressed medical imaging based on average sparsity model and reweighted analysis of multiple basis pursuit. *Comput. Med. Imaging Graph.* 90, 101927.
- Ranzato, M., Mnih, V., Hinton, G.E., 2010. Generating more realistic images using gated MRF's. In: Advances in Neural Information Processing Systems. pp. 2002–2010.
- Ratner, A.J., Ehrenberg, H., Hussain, Z., Dunnmon, J., Re, C., 2017. Learning to compose domain-specific transformations for data augmentation. In: Advances in Neural Information Processing Systems. pp. 53–63.
- Salahuddin, Z., Woodruff, H.C., Chatterjee, A., Lambin, P., 2022. Transparency of deep neural networks for medical image analysis: A review of interpretability methods. *Comput. Biol. Med.* 140, 105111.
- Shi, Z., Liu, M., Cao, Q., Ren, H., Luo, T., 2019. A data augmentation method based on cycle-consistent adversarial networks for fluorescence encoded microsphere image analysis. *Signal Process.* 161, 195–202.
- Szegedy, C., Vanhoucke, V., Ioffe, S., Shlens, J., Wojna, Z., 2016. Rethinking the inception architecture for computer vision. In: CVPR. IEEE, pp. 2818–2826.
- Telea, A., 2004. An image inpainting technique based on the fast marching method. *J. Graph. Tools* 9 (1), 25–36.
- Velden, B.H., Kuijf, H.J., Gilhuijs, K.G., Viergever, M.A., 2022. Explainable artificial intelligence (XAI) in deep learning-based medical image analysis. *Med. Image Anal.* 79, 102470.
- Wang, C.-W., Chang, C.-C., Lee, Y.-C., Lin, Y.-J., Lo, S.-C., Hsu, P.-C., Liou, Y.-A., Wang, C.-H., Chao, T.-K., 2022. Weakly supervised deep learning for prediction of treatment effectiveness on ovarian cancer from histopathology images. *Comput. Med. Imaging Graph.* 99, 102093.
- Xu, H., Li, C., Rahaman, M.M., Yao, Y., Li, Z., Zhang, J., Kulwa, F., Zhao, X., Qi, S., Teng, Y., 2020. An enhanced framework of generative adversarial networks (EF-GANs) for environmental microorganism image augmentation with limited rotation-invariant training data. *IEEE Access* 8, 187455–187469.
- Yang, F., Liang, F., Lu, L., Yin, M., 2022. Dual attention-guided and learnable spatial transformation data augmentation multi-modal unsupervised medical image segmentation. *Biomed. Signal Process. Control* 78, 103849.
- Yu, X., Wang, J., Hong, Q.-Q., Teku, R., Wang, S.-H., Zhang, Y.-D., 2022. Transfer learning for medical images analyses: A survey. *Neurocomputing* 489, 230–254.
- Zaman, A., Park, S.H., Bang, H., woo Park, C., Park, I., Joung, S., 2020. Generative approach for data augmentation for deep learning-based bone surface segmentation from ultrasound images. *Int. J. Comput. Assist. Radiol. Surg.* 15, 931–941.
- Zhao, J., Sun, L., Zhou, X., Huang, S., Si, H., Zhang, D., 2022. Residual-atrous attention network for lumbosacral plexus segmentation with MR image. *Comput. Med. Imaging Graph.* 102109.